RESEARCH ARTICLE

ADVANCED OPTICAL MATERIALS
www.advopticalmat.de

Visualizing 3D Anisotropic Molecular Orientation in Polarization Holographic Optical Elements via Dielectric Tensor Tomography

Juheon Lee, Heeju Son, Seung Jae Hong, Herve Hugonnet, Joona Bang, Seungwoo Lee, and YongKeun Park**

The ability to unveil the spatial distribution of refractive index (RI) within volumetric holographic optical elements (HOEs) is critical for quantitating their diffractive behaviors. Angle-resolved far-field measurements of diffractive intensity have been prevalent toward this end. However, this century-old approach is unable to directly visualize the spatial distribution of RI at mesoscopic scale. More significantly, visualization of molecular orientation within photoaddressable polymers (PAPs), which serve as standard recording media for polarization HOEs (pHOEs), remains uncharted territory. The recent advent of dielectric tensor tomography (DTT) has paved the way for full characterization of 3D anisotropic dielectric tensors, encompassing principal RIs and their optic axes. This study embarks on direct visualization of the 3D spatial distribution of anisotropic molecular orientations within holographically recorded PAPs. Illuminating these PAPs with polarized light at varying angles, the diffracted vector fields essential for reconstructing the dielectric tensor tomogram are captured. After diagonalizing the dielectric tensors, periodic rotations of the anisotropic molecule orientations can be visualized in the PAPs, which have never been achieved so far. The homogeneity of grating patterns produced under diverse manufacturing conditions is also examined and juxtaposed.

1. Introduction

Holographic optical elements (HOEs) are century-old media, playing critical roles across various sectors such as 3D imager, data storage, and augmented/virtual reality displays.[1] For a holographic recording of conventional HOEs, intensity interference pattern (IIP), where an electric field with a consistent polarization is sinusoidally modulated along the grating vector, can be directly encoded in a volumetric media, for example, by intensity-proportional photopolymerization. Thus, with respect to the geometry of IIP, material density and the resultant refractive index (RI) are volumetrically modulated in HOEs without the encoding of polarization information. By contrast, polarization HOEs (pHOEs) hold a promise as Bragg diffractive media with which to encode the polarization information in volume gratings. Photoaddressable polymers (PAPs) have been the gold vistas of pHOE media toward this end. In particular, the long axis of azobenzene molecules

J. Lee, H. Hugonnet, Y. Park
Department of Physics
Korean Advanced Institute of Science and Technology (KAIST)
Daejeon 34141, Republic of Korea
E-mail: yk.park@kaist.ac.kr

J. Lee, H. Hugonnet, Y. Park
KAIST Institute for Health Science and Technology
KAIST
Daejeon 34141, Republic of Korea

H. Son, S. Lee
KU-KIST Graduate School of Converging Science and Technology
Korea University
Seoul 02841, Republic of Korea
E-mail: seungwoo@korea.ac.kr

S. J. Hong, J. Bang
Department of Chemical and Biological Engineering
Korea University
Seoul 02841, Republic of Korea

S. Lee
Department of Biomicrosystem Technology
Korea University
Seoul 02841, Republic of Korea

S. Lee
Department of Integrative Energy Engineering and KU Photonics Center
Korea University
Seoul 02841, Republic of Korea

S. Lee
Center for Opto-Electronic Materials and Devices
Post-Silicon Semiconductor Institute
Korea Institute of Science and Technology (KIST)
Seoul 02792, Republic of Korea

Y. Park
Tomocube Inc.
Daejeon 34109, Republic of Korea

The ORCID identification number(s) for the author(s) of this article can be found under https://doi.org/10.1002/adom.202302346

DOI: 10.1002/adom.202302346

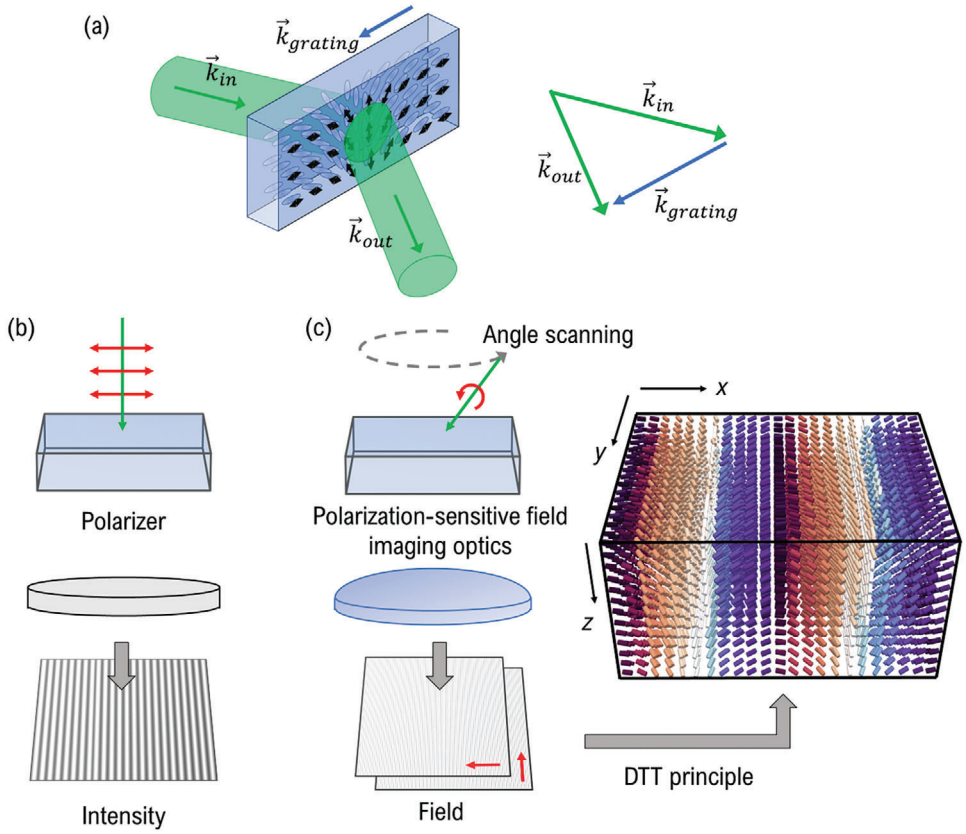

Figure 1. Investigative methodologies assessing pHOE. a) Diffraction of polarization volume gratings, with arrows highlighting the relationship between the Bragg angle and the grating vector $\vec{k}_{grating}$ where diffraction efficiency reaches its peak along the wavevector $\vec{k}_{out}$ in terms of the incident wavevector $\vec{k}_{in}$. b) Polarized light microscopy, where pattern quality is inferred from a 2D projected intensity image. c) DTT, in which the anisotropic structure of the grating is reconstructed in terms of DTT.

in PAPs can become aligned with respect to the vertical direction to the polarization of incoming light, in that illumination of polarization interference pattern (PIP), where the polarization is linearly rotated across the grating vector without change in intensity, gives rise to the volumetric encoding of the polarization information. Thus, the PIP-encoded RI modulation in pHOEs and the resultant diffractive efficiency (DE) can be polarization sensitive in contrast to those of HOEs and, by extension, can act as light modulator carrying the orbital angular momentum through a more sophisticated design such as the catenary structures.[2] Furthermore, PAPs are easy-to-craft in terms of developing a thick film, which enables an ultranarrow angular selectivity, promoting a vast number of multiplexing of volume gratings. More critically, the molecular orientations of azobenzene can be repeatably erased and rewritten (i.e., updatable volume hologram), which makes PAPs starkly contrasted with holographic photopolymers.

Either HOEs and pHOEs have dominantly depended on angle-resolved, far-field measurement of DE for qualitatively analyzing of the volumetrically modulated RI (**Figure 1a**).[3] Scatterometry, another method, assesses diffracted light to ascertain the dimensional parameters of grating structures.[4] Nevertheless, these methods are unable to characterize a microscopic spatial distribution of RI. Ellipsometry has been suggested as an alternative for HOE's RI and thickness measurement,[5] but this technique requires complex computations to derive parameters and lacks sensitivity to changes in the RI of HOEs. High-resolution imaging techniques like atomic force and scanning electron microscopy, which measure the surface grooves of HOEs, are not suitable for phase-modulated grating measurement.[6] Recently, several strategies have used an interferometric system to image phase-modulated HOEs. Phase contrast microscopy provides 2D contrast images of phase gratings.[7] Quantitative phase imaging (QPI) techniques exploit RI as an imaging contrast.[8] 2D QPI technique was used to demonstrate the measurements of 2D phase delay profiles of grating structures.[9] Polarization sensitive QPI techniques have been reported to measure 2D phase delay maps as a function of polarization states.[10] 3D QPI technique, also known as holotomography, reconstructs 3D RI distribution of a sample via tomographic reconstruction,[11] which can be used for the characterizations of HOEs. However, these methods fall short of measuring optically anisotropic 3D pHOEs structures. Nevertheless, all of these methods cannot quantitatively measure the regularly rotating molecular orientations of anisotropic azobenzene molecules, which have been reliant on speculation thus far.

Polarization-sensitive imaging techniques are indispensable for pHOE quantitation, given that their grating patterns are formed by rotating the optic axis of anisotropic material. Polarized light microscopy is a conventional technique offering polarization-sensitive contrast images of anisotropic structures

(Figure 1b).[12] However, this method is limited to 2D plane information. Other methods extend the principle of optical diffraction tomography to display 3D polarization-sensitive contrast,[13] but these necessitate strict sample assumptions for complete anisotropy reconstruction. Recently, dielectric tensor tomography (DTT), a technique enabling volumetric 3D anisotropic structure measurement, has emerged (Figure 1c).[14] The optical anisotropy can be fully characterized by inversely solving the vector wave equation, which includes 3D principal RI distributions and their optic axes with a microscopic resolution.

This study presents the direct visualization of the holographically modulated molecular directors within a volumetric pHOEs using DTT. The 1D polarization volume gratings were recorded by illuminating the pHOEs with a PIP. The dielectric tensor tomograms were reconstructed from the measured fields, based on the DTT principle. Periodic rotation of anisotropic molecular orientations in the grating volume was directly visualized by diagonalizing the dielectric tensors, which were out of reach for the last century. Further, we evaluated and compared the homogeneities of the measured polarization volume gratings under various sample conditions.

2. Experimental Section

2.1. Holographic Inscription of pHOEs

The pHOEs were developed using a PAP, specifically polymethylmethacrylate (PMMA)-b-P(liquid crystalline (LC)-r-azobenzene (Azo)), synthesized through atom transfer radical polymerization (**Figure 2a**). The polymer was then sandwiched between two cover glasses with 60 μm spacers, as outlined in the previous work.[15] This PAP can be divided into two main parts: i) Azo/LC side groups serving as photochromic reactive moieties; ii) PMMA acting as an optically transparent host medium, crucial for the casting of thick polymer films.

On light exposure, the azobenzene molecules within the polymeric host underwent repetitive trans–cis–trans isomerization cycles. This isomerization cycles cease when the long-axis of trans isomer becomes accidentally aligned perpendicularly to the polarization state, resulting in a molecular orientation.[16] These photoinduced molecular alignments in Azo drive the cooperative motions that enable the surrounding LC side groups to align along the long axis of neighboring Azo side groups. This process amplifies birefringence even in a volumetric thick film; promoting volume modulation of RI.[17] Therefore, by illuminating the PIP, a polarization volume hologram with the desired anisotropic structure can be inscribed.

The PIP was generated by mixing two incident beams with left-circular polarization (LCP) and right-circular polarization (RCP).[15] The total electric field E can be described as follows:

$$E = \exp\left(i\frac{2\pi}{\lambda}xsin\theta\right)\ \left(\vec{p}_1 + \vec{s}\right) + \exp\left(-i\frac{2\pi}{\lambda}xsin\theta\right)\ \left(\vec{p}_2 - \vec{s}\right)$$
$$= \begin{pmatrix} 2\cos(\theta)\cos\left(\frac{2\pi}{\lambda}xsin\theta\right) \\ -2sin\left(\frac{2\pi}{\lambda}xsin\theta\right) \\ 2isin(\theta)\,sin\left(\frac{2\pi}{\lambda}xsin\theta\right) \end{pmatrix} \quad (1)$$

$$\vec{s} = \hat{y},\ \ \vec{p}_1 = \cos(\theta)\ \hat{x} + \sin(\theta)\,\hat{z},\ \ \vec{p}_2 = \cos(\theta)\ \hat{x} - \sin(\theta)\,\hat{z} \quad (2)$$

where θ, λ, and $\vec{s}$ are the incident angle, the wavelength, and the polarization state perpendicular to the incident plane, respectively. $\vec{p}_1$ and $\vec{p}_2$ are the polarization states parallel to the incident plane for each incident beam. Note that the phase delay i at the z component indicates elliptical polarization, and normal axes of the elliptical polarizations are rotated along the x direction with a period of $0.5\lambda/sin\theta$ (Figure 2b). Prepared samples were illuminated with 532 nm wavelength PIP at an incident angle of 15.5°, forming regularly rotating molecular directors of Azo/LC with a period of 1 μm.

Four variants of pHOEs were prepared with varying ratios of moieties and exposure times (**Table 1**). To explore the effects of azobenzene content and laser exposure, the weight percentage of the azo group was adjusted to either 7 or 18 wt.%, with laser exposure durations of 2, 10, and 30 min.

2.2. Dielectric Tensor Tomography

The optical system, based on a Mach–Zehnder interferometer with spatially multiplexed off-axis holography, was constructed as shown in Figure 2c.[14,18] The laser source (wavelength λ = 532 nm; Cobolt AB) was divided into a sample and reference arm using a beam splitter. A digital micromirror device (DLi 4130, Digital Light Innovations) was employed in the sample arm for rapid control of the sample illumination angles.[19] Then, a LC retarder (LCC1223-A, Thorlabs) was used to control the illumination polarization. A 4-f system, along with a condenser lens (UPLSAPO 60XW, Olympus), was employed over the sample to enable high angle illumination, and diffracted fields were collected using an objective lens (UPLSAPO 60XW, Olympus), and a tube lens. The gathered beam was combined with two perpendicularly polarized reference beams, formed using a Wollaston prism. As the light with perpendicular polarization does not interfere, two polarization-dependent holograms were generated, forming a check pattern on the image sensor (Lt425R, Lumenera).

For DTT reconstruction, the multiplexed holograms were recorded at various illumination angles (Figure 2d). For each multiplexed hologram, the polarization-sensitive fields were simultaneously extracted based on the off-axis holography method.[20] The measured fields were vectorized in Cartesian coordinates and combined to reconstruct the dielectric tensor tomograms based on the DTT principle.[14] To remove speckle noise caused by dust and low signal to noise ratio in the sample, the six tensor tomograms were filtered in the Fourier domain during the reconstruction process,

$$\overleftrightarrow{\tilde{\epsilon}}_{ij}^{\,\text{filtered}} = F\overleftrightarrow{\tilde{\epsilon}}_{ij} \quad (3)$$

where the binary filtering mask F was generated by thresholding the Fourier domain depending on the value of the L_1-norm of the dielectric tensor, which includes integrated information ≈ all tensor elements (Figure 2e). As shown, this removed noise while keeping harmonic frequency terms due to the periodic grating structure. In Figure 2f, the individual components of the filtered dielectric tensor are visualized. It is important to note that, as the

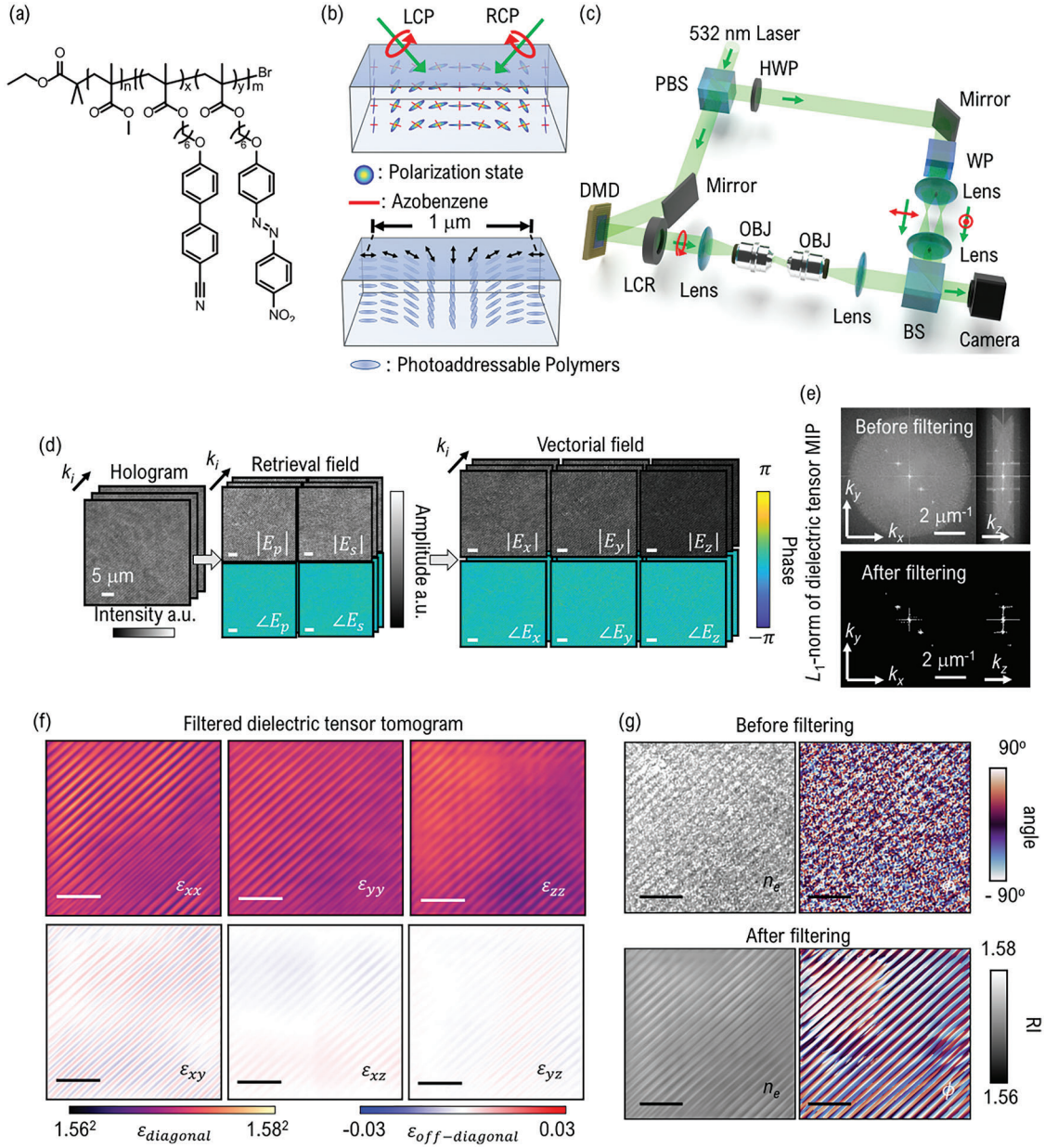

Figure 2. Measurements of the DTT of pHOE samples. a) Chemical structures of PaPs. b) Preparation of the pHOEs. The grating consists of a block copolymer including Azo side groups with liquid crystals. Under the interference pattern of left and right circular polarization beams, the Azo side groups and liquid crystal were aligned in the orientations linearly rotated along the lateral direction. c–g) Data acquisition in the DTT. c) The experimental setup for DTT is based on the Mach-Zehnder interferometry. d) Recorded holograms at various illumination angles, retrieved fields, and vectorized fields in the Cartesian coordinates. e) *L1*-norm of the dielectric tensor tomogram in the Fourier domain, before and after Fourier filtering. f) Six elements of the dielectric tensor tomogram after the Fourier filtering. g) Orientation angles, extraordinary RI, and ordinary RI before and after the Fourier filtering, acquired by diagonalizing the dielectric tensor tomogram.

dielectric tensor is symmetric, six components of the tensor were reconstructed, and the remaining components were deduced. The dielectric tensor tomograms were diagonalized based on the singular value decomposition method to visualize the principal RIs and their optic axes. In Figure 2g, the extraordinary RI and lateral angle of orientations were visualized, comparing results before and after filtering. The theoretical spatial resolution of the imaging system stands at 111 nm in the lateral direction and 453 nm in the axial direction, respectively.[21]

3. Results and Discussion

To visualize the birdeye-viewed molecular orientations of the pHOEs, we imaged the polarization volume gratings with a size

Table 1. Sample conditions depending on the weight percentage of compositions and laser exposure time.

Sample number	$AzoNO_2$ [wt.%]	LC [wt.%]	PMMA [wt.%]	Laser exposure time [min.]
1	7	59	34	10
2	18	50	32	2
3	18	50	32	10
4	18	50	32	30

of 212 × 212 × 21.2 µm (sample 3), by stitching 5 × 5 tiled images. **Figure** 3a shows the resulting stitched image visualizing the regularly rotating molecular directors of the Azo and LC side group moieties. This method enabled visualization of a large part of the sample in which the large area polarization gratings were fully inscribed along the volumetric thick film. A zoom-in 10 × 10 × 10 µm (Figure 3b) and 2 × 2 × 2 µm (Figure 3c) views of the grating pattern taken at azimuthal angles further detailed the spatial distributions of anisotropic molecular directors. In particular, the anisotropic molecular directors rotate periodically along the grating vector with a period of ≈ 1 µm, which shows good agreement with the vertical counterpart of the polarization pattern in PIP. The corresponding cross-sections of molecular alignment were extracted in the *x'z* plane and *x'y'* plane centered around the y' axis and z axis respectively (Figure 3d,e). In Figure 3d, while exhibiting a slight tilt of molecules as depth increases along the *z* direction, the molecules are aligned predominantly maintaining the alignment in the upper region. In the *x'y'* plane, the linear rotations of the molecules matched with the polarization directions of the PIP are illustrated in accordance with periodicity shown in Figure 3e.

We proceeded to develop a quantitative analysis of the grating structure, with initial evaluation conducted on Sample 4, crafted with a high percentage of the Azo group and exposed to prolonged laser exposure. Displayed in **Figure** 4a are cross-sectional images of the measured principal RIs n_e and n_o along with the azimuthal angles of the optic axes. Consistent with the intended grating pattern, the optic axes were observed to rotate linearly along the *x* direction. However, an unexpected spatial inhomogeneity was found in the measured principal RIs n_e and n_o. This discrepancy may have arisen due to unintentional spatial changes in the PIP intensity, caused potentially by diffraction and absorption effects induced by pre-inscribed gratings near the upper surface.

To enhance the clarity of visual interpretation, we incorporated zoomed-in 3D rendering images, showcasing molecular alignments (Figure 4b). The specific regions magnified are indicated by red lines in Figure 4a. Each horizontal cross-section presents linear rotation of the optic axes. Nevertheless, slight phase discrepancies were observed in the periodic patterns across different sections, which may have been due to the absorption and scattering of PIP at the upper surface.

In order to quantitatively evaluate these observed molecular misalignments, we performed a statistical analysis of the orientations of the optic axes. Figure 4c presents line profiles of the optic axis angle along the *x* directions, with the statistical analysis

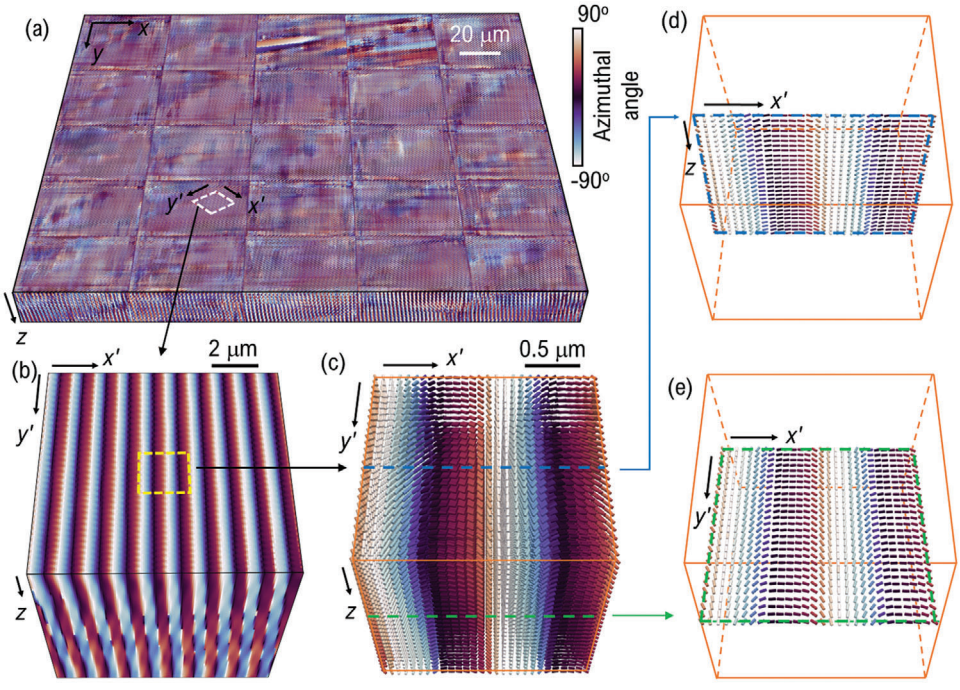

Figure 3. Visualization and analysis of pHOE based on DTT. a) Wide-field image of optic axis orientations acquired using DTT. The image was compiled by stitching together 25 (5 × 5) tiled images. b) Enlarged detailed images from a selected area within the wide-field image (outlined by a white dashed box). c) 3D visualization of optic axes extracted from a specific area (indicated by a yellow dashed box). d,e) Highlighted cross-sections of *x'y'* (marked by a green line) and *x'z* (marked by a blue line).

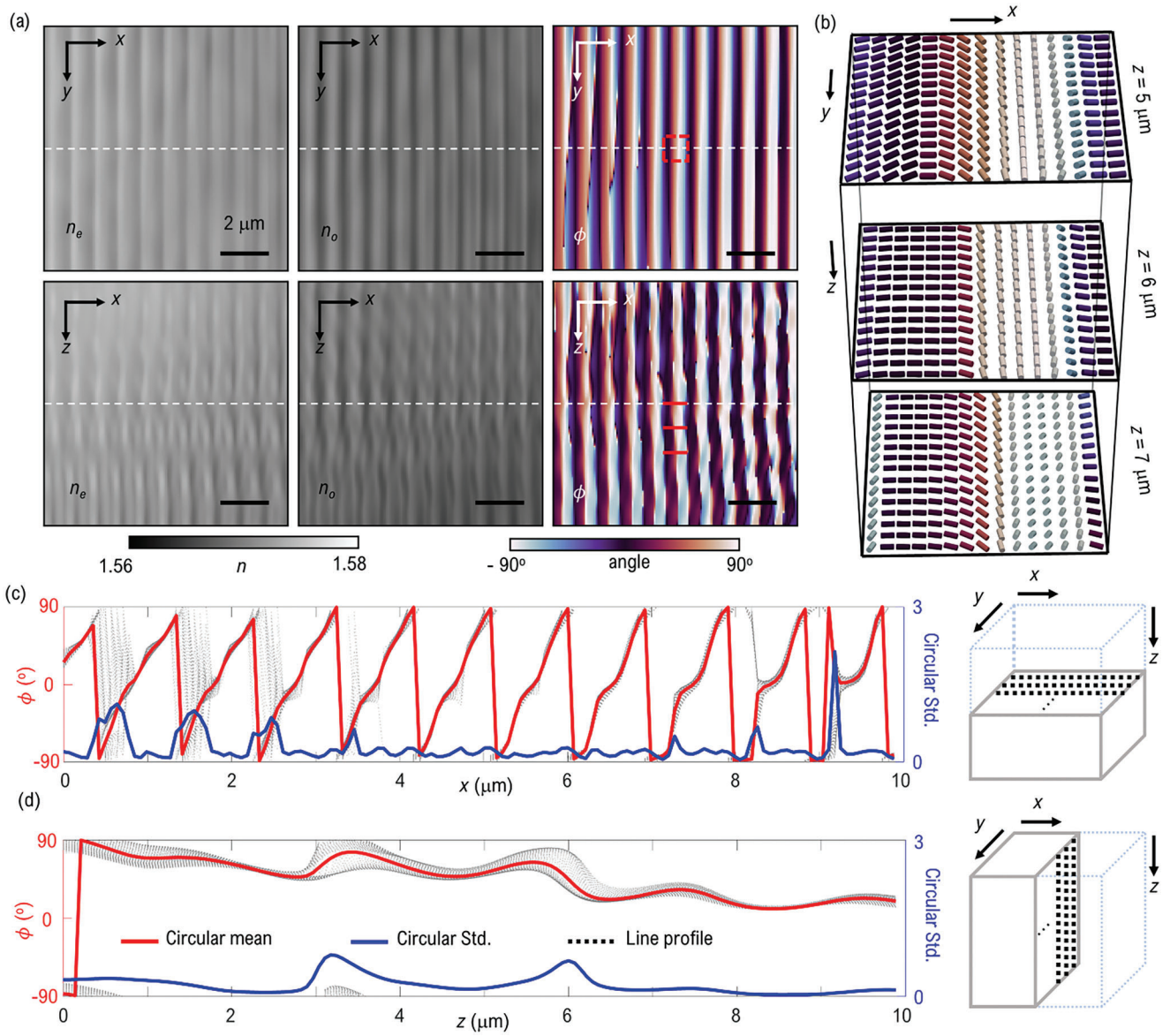

Figure 4. a) Cross-section images of n_e (extraordinary RI), n_o (ordinary RI), and orientation angle of optic axis. The white dashed lines indicate positions of the cross-sections. b) 3D view of the optic axes in the magnified region. The visualized cross-sections correspond to the red lines in (a). c, d) Plot of line profiles with their circular mean and standard deviation along the x and z directions. The dotted lines in the right schematic indicate positions of the line profiles within the tomogram. The red and blue lines indicate the circular mean and standard deviations of the line profiles, respectively.

being conducted at the central z section of the measured tomogram. Here, we calculated the circular mean and standard deviation of the angles using directional statistics as,[22]

$$\bar{\phi} = \frac{1}{2}\arg\left(\frac{1}{n}\sum_k e^{2i\phi_k}\right),\ \sigma_\phi = \sqrt{-2\ln\left(\left|\frac{1}{n}\sum_k e^{2i\phi_k}\right|\right)} \quad (4)$$

In these equations, the azimuthal angle ϕ is wrapped in terms of phase values in the complex exponential function before averaging. The angle of the averaged complex value is termed the circular mean, while the magnitude of this averaged complex value determines the circular standard deviation. In this context, a value of 0 signifies no deviation, and a value approaching infinity indicates a random distribution. As illustrated in the graphs, the mean angle of the optic axes exhibits a linear oscillation between −90° and 90°. However, the standard deviation along the x direction presents a periodic fluctuation, with an increase near the 90° angle, which is perpendicular to the grating vector. This observation can be attributed to the fact that the polarization states of the PIP at this juncture become linear. As per Equation 1, the z component of the PIP field periodically approaches zero, aligning with the y component. Consequently, the orientation of the Azo group, which aligns perpendicular to polarization, becomes undefined.

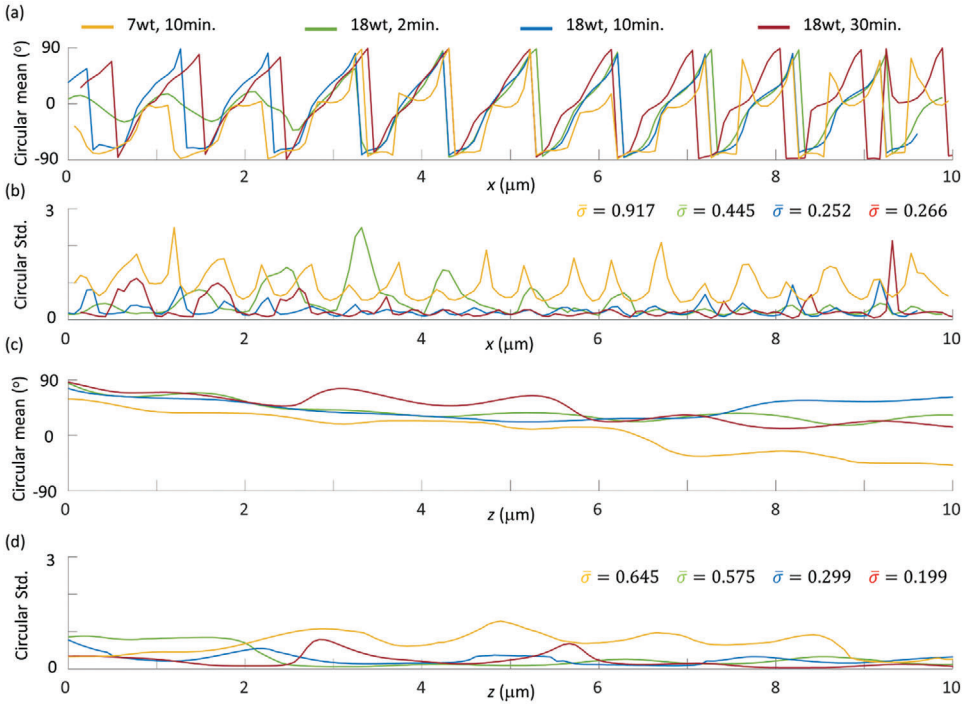

Figure 5. Directional statistics under the sample conditions. Each sample is represented with distinct colors to signify corresponding information. a,c) Plot of circular mean along the *x* and *z* directions. b, d) Plot of circular standard deviation along the *x* and *z* directions. Values of individual average standard deviations are displayed in the top right corner of each graph.

Figure 4d presents line profiles of the optic axis angle along the *z* direction, along with their mean and standard deviation. As indicated in Figure 4b, the mean angles display a linear rotation along the *z* direction. With increasing the depth along the *z*-direction, the average rotation angles of molecules increase progressively. Due to the natural property of the Azo group which can absorb the light at 532 nm, the PIP cannot be reached into the deeper region along the *z* direction with sufficient intensity and intact formation of interference patterns. Thus, the molecules align with gradually rotated angles at deeper positions along the *z* direction.

In order to draw comparisons between different sample conditions, we carried out a comprehensive quantitative analysis. **Figure** 5a,c display the circular means along the *x* and *z* directions, respectively. Meanwhile, Figure 5b,d presents the circular standard deviations along with their respective average values. These metrics were crucial in assessing the homogeneity of the samples.

Upon scrutinizing the circular mean graphs along the *x* direction, it was found that all the samples exhibited linear rotations along the grating direction (Figure 5a). Viewing from the contents of the Azo group, sample 1 with low Azo content shows a decrease in the periodic homogeneity with the highest mean value of standard deviation ($\bar{\sigma} = 0.917$), relative to other samples with high content of Azo group. The overall molecular alignments of sample 1 are compromised due to the limited number of molecules which can be aligned by polarized light. In the case of 18 wt.% Azo-contained samples from sample 2 to sample 4, generally, they show that extended laser exposure durations correlate with enhanced molecular alignments, leading to reduction in the standard deviation and their mean values shown in Figure 5b.

Similar tendencies are discernible in the graphs oriented along the *z* direction. Figure 5c presents that the linear rotations of molecules are greater in sample 1 than in the samples with high content of Azo groups. Despite the high depth of light penetration of sample 1 due to the low concentration of Azo groups absorbing at 532 nm, the limitation in the number of Azo molecules induced misalignments by molecular rotations across the thickness throughout the sample with the maximum average standard deviation at 0.645. For sample 2 through sample 4, there is a reduction in the average values of molecular rotation along the z direction. The molecular oscillations can occur due to the continuous molecular reorientation caused by the alteration of PIP by initially formed diffraction patterns near the surface. However, with an increasing depth attainable by PIP, molecular alignments in the z direction become more precise, giving rise to notable reduction of mean deviation values from 0.575 to 0.199 (Figure 5d).

4. Conclusion

In this study, we have successfully demonstrated the three-dimensional measurements of anisotropic structures present in pHOEs, leveraging the capabilities of DTT. Our results have facilitated the straightforward visualization of the orientation of aligned molecules not only in the plane direction but also along the thickness direction of the samples. The architectures measured were found to align well with the intended design of the PIP. Moreover, we undertook a comparative analysis of the grating patterns fabricated under various conditions. Specifically, the

results highlighted the impact of the content of the Azo group and laser exposure duration on the quality of the resultant patterns. The findings provide crucial insights for the optimization of manufacturing parameters in future pHOE fabrication.

Despite these advancements, our study was not without limitations. One of the prominent challenges was the need to increase imaging depth by reducing speckle noise. The use of a coherent light source in the proposed method makes the DTT measurements susceptible to scatterers like dust, which can reduce imaging depth and quality. While Fourier filtering was employed in the reconstruction process to mitigate speckle noise, this approach may also inadvertently eliminate information about local defects in the pHOEs. In our future endeavors, we aim to address these issues by refining the processing algorithms to account for multiple scattering and by developing a novel DTT setup based on an incoherent illumination.

To sum up, the present work paves the way for more comprehensive and accurate analyses of anisotropic structures, promising significant advancements in the fabrication and evaluation of pHOEs, thereby broadening their application horizons. The versatility of DTT in being able to measure any anisotropic samples in 3D domain opens the door to a multitude of applications. Beyond quality evaluation of polarization volume gratings, this approach can potentially be employed to examine a wider array of complex anisotropic structures, which could prove beneficial in fields such as materials science, photonic devices, and biological research.[23]

Acknowledgements

This work was supported by National Research Foundation of Korea (NRF) grant funded by the Korea government (MSIT) (2015R1A3A2066550, NRF-2022M3H4A1A02074314, NRF-RS-2023-00272363, 2022R1A4A1020543), Institute of Information & communications Technology Planning & Evaluation (IITP) grant funded by MSIT (2021-0-00745), KAIST Institute of Technology Value Creation, Industry Liaison Center (G-CORE Project) grant funded by MSIT (N10240002), Samsung Research Funding & Incubation Center for Future Technology grant (SRFC-MA2301-20), the KIST Institutional Program (Project No.: 2V09840-23-P023), and Korea University grant.

Conflict of Interest

The authors declare no conflict of interest.

Data Availability Statement

The data that support the findings of this study are available from the corresponding author upon reasonable request.

Keywords

birefringence, dielectric tensor, gratings, holographic optical elements, holotomography, polarization, quantitative phase imaging

Received: September 21, 2023
Revised: February 16, 2024
Published online: March 3, 2024

[1] a) J. Ashley, M. P. Bernal, G. W. Burr, H. Coufal, H. Guenther, J. A. Hoffnagle, C. M. Jefferson, B. Marcus, R. M. Macfarlane, R. M. Shelby, G. T. Sincerbox, *IBM J. Res. Dev.* **2000**, *44*, 341; b) K. Hong, J. Yeom, C. Jang, J. Hong, B. Lee, *Opt. Lett.* **2014**, *39*, 127; c) W. C. Sweatt, *J. Opt. Soc. Am.* **1977**, *67*, 803; d) H.-J. Yeom, H.-J. Kim, S.-B. Kim, H. Zhang, B. Li, Y.-M. Ji, S.-H. Kim, J.-H. Park, *Opt. Express* **2015**, *23*, 32025; e) J. Xiong, K. Yin, K. Li, S.-T. Wu, *Advanced Photonics Research* **2021**, *2*, 2000049; f) D. Cheng, Q. Wang, Y. Liu, H. Chen, D. Ni, X. Wang, C. Yao, Q. Hou, W. Hou, G. Luo, *Light: Advanced Manufacturing* **2021**, *2*, 350.

[2] a) M. Pu, X. Li, X. Ma, Y. Wang, Z. Zhao, C. Wang, C. Hu, P. Gao, C. Huang, H. Ren, X. Li, F. Qin, J. Yang, M. Gu, M. Hong, X. Luo, *Sci. Adv.* **2015**, *1*, e1500396; b) Y. Wen, Q. Zhang, Q. He, F. Zhang, L. Xiong, F. Zhang, G. Fu, J. Xu, M. Pu, X. Luo, *Adv. Opt. Mater.* **2023**, *11*, 2300127.

[3] a) A. M. Cox, R. D. Blackburn, D. P. West, T. A. King, F. A. Wade, D. A. Leigh, *Appl. Phys. Lett.* **1996**, *68*, 2801; b) D. M. Chambers, G. P. Nordin, S. Kim, *Opt. Express* **2003**, *11*, 27; c) P.-A. Blanche, P. Gailly, S. Habraken, P. Lemaire, C. Jamar, *Optical Engineering* **2004**, 43.

[4] a) C. J. Raymond, M. R. Murnane, S. L. Prins, S. Sohail, H. Naqvi, J. R. McNeil, J. W. Hosch, *J Vac Sci Technol B: Microelectronics and Nanometer Structures Processing, Measurement, and Phenomena* **1997**, *15*, 361; b) M. H. Madsen, P.-E. Hansen, *Surface Topography: Metrology and Properties* **2016**, *4*, 023003.

[5] a) H. Tompkins, E. A. Irene, *Handbook of ellipsometry*, 1st ed, William Andrew, XX **2005**, 886. b) R. M. A. Azzam, N. M. Bashara, *Phys. Rev. B* **1972**, *5*, 4721; c) C. Röling, P. Thiesen, A. Meshalkin, E. Achimova, V. Abashkin, A. Prisacar, G. Triduh, *J. Non-Cryst. Solids* **2013**, *365*, 93.

[6] a) M. Jergel, P. Mikulík, E. Majková, S. Luby, R. Senderák, E. Pincík, M. Brunel, P. Hudek, I. Kostic, A. Konecníková, *J. Phys. D: Appl. Phys.* **1999**, *32*, A220; b) J. Garnaes, P. E. Hansen, N. Agersnap, J. Holm, F. Borsetto, A. Kühle, *Appl. Opt.* **2006**, *45*, 3201.

[7] a) R. K. Kostuk, J. W. Goodman, *Appl. Opt.* **1991**, *30*, 369; b) I. Bányász, *Appl. Phys. Lett.* **2003**, *83*, 4282.

[8] a) Y. Park, C. Depeursinge, G. Popescu, *Nat. Photonics* **2018**, *12*, 578; b) V. Balasubramani, M. Kujawińska, C. Allier, V. Anand, C.-J. Cheng, C. Depeursinge, N. Hai, S. Juodkazis, J. Kalkman, A. Kuś, *Journal of Imaging* **2021**, *7*, 252.

[9] a) M. d. Angelis, S. D. Nicola, A. Finizio, G. Pierattini, P. Ferraro, S. Pelli, G. Righini, S. Sebastiani, *Appl. Phys. Lett.* **2006**, *88*, 111114; b) V. Cazac, A. Meshalkin, E. Achimova, V. Abashkin, V. Katkovnik, I. Shevkunov, D. Claus, G. Pedrini, *Appl. Opt.* **2018**, *57*, 507; c) C. Zheng, D. Jin, Y. He, H. Lin, J. Hu, Z. Yaqoob, P. T. So, R. Zhou, *Advanced Photonics* **2020**, *2*, 065002.

[10] a) Y. Kim, J. Jeong, J. Jang, M. W. Kim, Y. Park, *Opt. Express* **2012**, *20*, 9948; b) J. Park, H. Yu, J.-H. Park, Y. Park, *Opt. Express* **2014**, *22*, 24304; c) S. Shin, K. Lee, Z. Yaqoob, P. T. So, Y. Park, *Opt. Express* **2018**, *26*, 26858; d) Z. Wang, L. J. Millet, M. U. Gillette, G. Popescu, *Opt. Lett.* **2008**, *33*, 1270; e) B. Ge, Q. Zhang, R. Zhang, J.-T. Lin, P.-H. Tseng, C.-W. Chang, C.-Y. Dong, R. Zhou, Z. Yaqoob, I. Bischofberger, P. T. C. So, *ACS Photonics* **2021**, *8*, 3440.

[11] a) K. Kim, J. Yoon, Y. Park, *Opt. Lett.* **2016**, *41*, 934; b) E. Wolf, *Opt. Commun.* **1969**, *1*, 153; c) Y. He, Q. Shao, S.-C. Chen, R. Zhou, *Addit. Manuf.* **2022**, *60*, 103293.

[12] V. Cazac, E. Achimova, V. Abashkin, A. Prisacar, C. Loshmanschii, A. Meshalkin, K. Egiazarian, *Opt. Express* **2021**, *29*, 9217.

[13] a) J. van Rooij, J. Kalkman, *Biomed. Opt. Express* **2020**, *11*, 2109; b) A. Saba, J. Lim, A. B. Ayoub, E. E. Antoine, D. Psaltis, *Optica* **2021**, *8*, 402.

[14] S. Shin, J. Eun, S. S. Lee, C. Lee, H. Hugonnet, D. K. Yoon, S.-H. Kim, J. Jeong, Y. Park, *Nat. Mater.* **2022**, *21*, 317.

[15] K. Kim, Y. Lim, H. Son, S. J. Hong, C.-W. Shin, D. Baek, H. H. Kim, N. Kim, J. Bang, S. Lee, *Adv. Opt. Mater.* **2022**, *10*, 2201421.

[16] K. Christian, R. Michael, S. Joachim, *J. Phys.: Condens. Matter* **2003**, *15*, S813.
[17] a) A. Natansohn, P. Rochon, *Chem. Rev.* **2002**, *102*, 4139; b) M. Ishiguro, D. Sato, A. Shishido, T. Ikeda, *Langmuir* **2007**, *23*, 332; c) A. Saishoji, D. Sato, A. Shishido, T. Ikeda, *Langmuir* **2007**, *23*, 320.
[18] J. Lee, S. Shin, H. Hugonnet, Y. Park, *Opt. Lett.* **2022**, *47*, 6205.
[19] a) S. Shin, K. Kim, J. Yoon, Y. Park, *Opt. Lett.* **2015**, *40*, 5407; b) K. Lee, K. Kim, G. Kim, S. Shin, Y. Park, *Opt. Lett.* **2017**, *42*, 999.
[20] a) M. Takeda, H. Ina, S. Kobayashi, *J. Opt. Soc. Am.* **1982**, *72*, 156; b) A. W. Lohmann, *Appl. Opt.* **1965**, *4*, 1667.
[21] C. Park, S. Shin, Y. Park, *J. Opt. Soc. Am. A* **2018**, *35*, 1891.
[22] K. Mardia, P. Jupp, Wiley Series in Probability and Statistics, **2008**.
[23] a) L. H. Nicholls, F. J. Rodríguez-Fortuño, M. E. Nasir, R. M. Córdova-Castro, N. Olivier, G. A. Wurtz, A. V. Zayats, *Nat. Photonics* **2017**, *11*, 628; b) M. D. Shoulders, R. T. Raines, *Annu. Rev. Biochem.* **2009**, *78*, 929; c) L. Gianaroli, M. C. Magli, A. P. Ferraretti, A. Crippa, M. Lappi, S. Capitani, B. Baccetti, *Fertility and Sterility* **2010**, *93*, 807.